Journal of Applied Polymer Science

REVIEW

Flexible ITO-Free Polymer Solar Cells

Dechan Angmo, Frederik C. Krebs

Department of Energy Conversion and Storage, Technical University of Denmark, DK-4000 Roskilde, Denmark

Correspondence to: F. C. Krebs (E-mail: frkr@dtu.dk)

ABSTRACT: Indium tin oxide (ITO) is the material-of-choice for transparent conductors in any optoelectronic application. However, scarce resources of indium and high market demand of ITO have created large price fluctuations and future supply concerns. In polymer solar cells (PSCs), ITO is the single-most cost driving factor due to expensive raw materials and processing. Given the limited lifetime and stability of PSCs as compared with other mature technologies such as silicon-based solar cells, the technological future of PSCs beyond that of academic interests rests in reducing cost of production. In this regard, replacing ITO has the potential to dramatically reduce material and processing cost and the energy payback time of PSCs. Several alternatives to ITO are present but not all of them bring competitive advantage over ITO for application in PSCs. This review explores some potentially low-cost alternatives to ITO suitable for use in PSCs. These alternatives belong to four material groups: polymers; metal and polymer composites; metal nanowires and ultra-thin metal films; and carbon nanotubes and graphene. We further present the progress of employing these alternatives in PSCs and identify future challenges. © 2012 Wiley Periodicals, Inc. J. Appl. Polym. Sci. 129: 1–14, 2013

KEYWORDS: applications; conducting polymers; films

Received 4 October 2012; accepted 19 November 2012; published online 18 December 2012

DOI: 10.1002/app.38854

INTRODUCTION

Polymer solar cells (PSCs) is a dawning industry that bears the potential of a technology that could very well supplement other forms of renewable energy resources in quenching the world's thirst for increasing energy supply. In fact, PSCs have the potential to deliver energy at a cost that can compete with fossil fuels.[1] This promise of PSCs relies on low cost of materials and simple processing requirements. Low cost processing is envisioned through high throughput roll-to-roll (R2R) printing and coating methods known from the printing industry for magazines and newspapers. PSCs have therefore garnered increasing research interest over the last decade or so with publications increasing from a few hundred annually in the year 2000 to several thousands in the year 2011. Initially, the prime focus was in the optimization of the photoactive polymer to enable power conversion efficiencies that were meaningful in the context of global energy supply and in comparison with other solar energy conversion means. In this context, the facets that make PSCs an attractive technology, the use of low cost materials and simple processing conditions, were largely ignored and efforts were mostly concentrated on increasing power conversion efficiencies. Such efforts have indeed materialized with current power conversion efficiencies of PSCs reaching 10% (Mitsubishi) that brings PSCs on par with inorganic thin film photovoltaics. Now, the challenge lies in translating such an efficiency achieved on devices with an active area significantly less than 1 cm^2 (typically a few mm^2) to large area modules produced by R2R processing while ensuring that the low cost objective of PSCs is achieved.

It was not too long after the initial R2R experiments on PSCs and life cycle analyses studies that it became apparent that the use of indium tin oxide (ITO) and vacuum processing is not feasible for low cost production of PSCs. ITO is a commercially dominant transparent conductor with relatively high conductivity (sheet resistance of 10–20 $\Omega\square^{-1}$) and transmission (>80%) in the visible region of the solar spectrum. However, the scarcity of indium resources in the world and its high demand from the display industry has created large cost fluctuations and future supply concerns. An official report on the market trend of minerals United States Geological Survey (USGS) suggests that the price of indium increased by approximately 25% between 2010 and 2011 from $570/kg reaching a maximum of $780/kg in the U.S. while world-wide production of indium increased only by 5%.[2] The price of indium has fluctuated anywhere between 10 and 40% annually in the past 5 years.[2] Apart from the volatility of indium prices, its incorporation in the processing of ITO requires high preparation temperatures and vacuum-based highly energy intensive deposition techniques such as sputtering, thus further increasing the cost of ITO. Life cycle analyses (LCA) of R2R produced ITO-based PSC modules reveal that

Applied Polymer SCIENCE

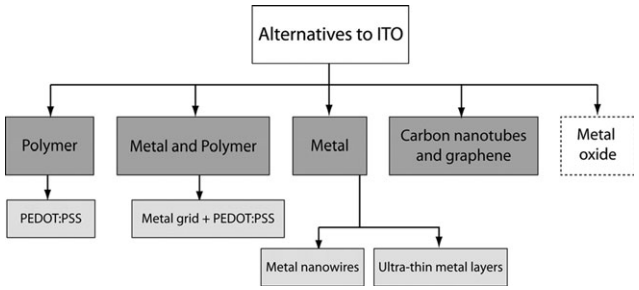

Figure 1. Alternatives to ITO as applied in polymer solar cells. Metal oxides are not included in this review as they bear no processing advantages over ITO (except perhaps in elemental abundance).

ITO on PET substrate account for ~90% of the total energy (embodied energy and direct process energy) imposed by all input raw materials.[3] Cost analyses[4–6] suggest that ITO accounts for >50% of the total cost of a PSC module and its replacement with cheaper alternative would significantly reduce the cost per watt and energy payback time (EPBT). For example, silver nanowires (AgNW) and highly conductive poly(3,4-ethylenedioxythiophene)-poly(styrenesulfonate) or PEDOT : PSS when used in place of ITO could potentially reduce cost per watt of PSC module up to 20% and energy payback time (EPBT) up to >30% in comparison with ITO-based PSC modules[4] and in the case of solution-processed ultra thin transparent metal conductor when used in PSCs, LCA studies indicate a potential reduction in EPBT of >50% even at half the PCE of ITO-based modules.[7] Apart from cost, ITO brings other disadvantages: its brittle nature limits flexibility as well as creates poor interfacial compatibility between the organic materials and the ITO surface[4,8,9] It is therefore crucial to find a low cost replacement to ITO that bears no supply concerns, is flexible, and is preferably solution-based and involves vacuum-free processing.

The alternatives of ITO could be categorized into four broad material groups: (1). polymer; (2). metal; (3). a combination of polymer and metal; and (4) carbon nanotubes and graphene (Fig. 1). These material groups are not mutually exclusive and are often used in some combination with each other. In this review, we elaborate on all four groups as they pertain to PSCs. Doped metal oxides form another group of alternatives for ITO but they bear no processing and property advantages (except perhaps in abundance) in comparison with ITO and are therefore not covered in this review. Many of the alternatives reported in literature are based on laboratory scale devices with less than a cm^2 of active area; hence, extrapolating their feasibility in the processing of large area modules is not justified. At the same time, such ideas could not altogether be rejected. A bridge remains to be built where such concepts are carried forward to demonstrate their feasibility in R2R processing of large area modules or in bench-top printing and coating processing equipment such as the example demonstrated by Dam and Krebs.[10] Currently, there remains a large gap between the performance obtained on laboratory devices (PCE of 10%) and that obtained on flexible, vacuum-free, R2R processed modules processed under ambient conditions (PCE <2%). Finally, it must be emphasized that the projected performance of PSCs with respect to power conversion efficiency and stability leaves very little margin to incorporate any high-end processing techniques. To make PSCs economically profitable, cost to performance ratio (W_p^{-1}) has to be kept minimal. With performance reaching saturation, reducing cost is the only way to make PSCs competitive with what is available on the market today.

ALTERNATIVES TO INDIUM TIN OXIDE FOR USE IN POLYMER SOLAR CELLS

Polymeric (Semi-)transparent Conductors

The most important advantage of polymeric transparent conductors is that they can be solution processed and therefore readily processed in a R2R set-up using the plethora of coating and printing techniques available.[11,12] PEDOT : PSS is the most widely used polymeric salt for this application where PEDOT is a conjugated polymer in its oxidized state carrying a positive charge and PSS is a polymer having deprotonated sulfonyl groups carrying a negative charge (Fig. 2). PSS is added to EDOT during polymerization as a charge balancing counter ion and to improve the inherently low solubility of PEDOT in aqueous medium. Several in-depth reviews on PEDOT : PSS in general are present.[13,14] In PSCs, PEDOT : PSS was first used as a interfacial buffer layer in the normal device structure to facilitate selective transport of holes to the ITO electrode and to reduce the surface roughness of ITO that otherwise could lead to electrical shorts. Later, PEDOT : PSS was employed as the hole collecting back electrode in inverted structures while ITO served as the front electrode. In the latter case, transmission of PEDOT : PSS is not a requirement and so the thickness of PEDOT : PSS can be maximized to increase conductivity. PEDOT : PSS is expected to follow the classical relationship of conductivity increase with increasing thickness reaching saturation at a finite film thickness.[14,15] On the other hand, transmission of PEDOT : PSS films follows the Beer-Lambert law where transmission and film thickness are inversely related. As a result, there is a tradeoff between transmission and conductivity which proved to be major obstacle when PEDOT : PSS is used as a replacement of ITO. Several reports

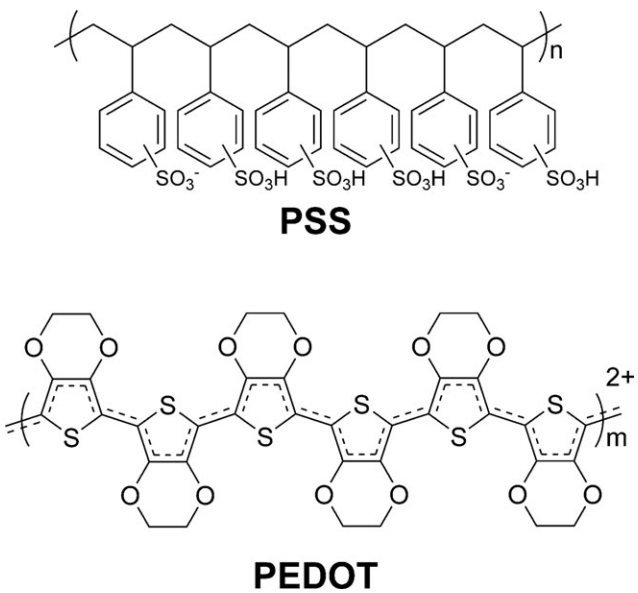

Figure 2. Chemical structure of PEDOT : PSS.

have delved into optimizing transmission and conductivity of PEDOT : PSS.[9,16] Particularly in earlier reports before the commercial availability of highly conductive formulations of PEDOT: PSS, such a trade-off between transmission and conductivity resulted in poor power conversion efficiencies of ITO-free PSCs and modules. In some cases, PEDOT : PSS having transmission in the range 10 to 30% (350–600 nm) for a comparable sheet resistance to ITO (10–20 $\Omega\square^{-1}$) have been reported.[17]

Therefore, the limiting factor of PEDOT : PSS films to be an efficient substitute for ITO is their conductivity. Originally, PEDOT : PSS had typical conductivity values around 1 to 10 S cm^{-1},[16,18] which was three orders of magnitude lower than that of ITO (>4000 S cm^{-1}) at similar transmission (80%). Increasing the inherent conductivity of PEDOT : PSS has generated successful results. Some of these methods include the addition of high boiling temperature polar compounds such as diethylene glycol,[19] ethylene glycol,[9,20] sorbitol,[21,22] dimethylsulfoxide (DMSO),[19,23,24] glycerol;[21,23,25] and by different chemistry methods such as controlling synthetic conditions, fundamental alteration of the polymer back bone, and by functionalizing the backbone with substituent side groups.[16] Several studies also looked into avoiding PSS that reduces the conductivity of PEDOT, by *in situ* oxidative polymerization of EDOT.[9,16,17] Most of these modifications of PEDOT : PSS have been substantiated with their positive influence on the photovoltaic properties of PSCs. Currently, highly conductive formulations of PEDOT : PSS are commercially available, for example, from Heraeus with the latest generations Clevious™ PH500 and PH1000 having a conductivity of 300 and 850 S cm^{-1}, respectively. This is in stark contrast to previous generations such as H.C. Stark Baytron P variants having sheet resistance 10^5 $\Omega\square^{-1}$ or 1–10 S cm^{-1}.

Earlier reports on PEDOT:PSS as replacement of ITO in PSCs were mostly in the context of poly[2-methoxy-5-(2-ethylhexyloxy)-1,4-phenylenenvinylene] or MEH-PPV and [6,6]-phenyl-C_{61}-butyric acid methyl ester (PCBM) based normal devices that employed first generation PEDOT : PSS.[20,21,26] These devices had lower performance than their ITO-based control devices. Subsequently, the use of highly conductive (hc)PEDOT : PSS such as PH500 as transparent conductor resulted in comparable performance to ITO-based control devices and a maximum power conversion efficiency (PCE) of 3.27%, open-circuit voltage (V_{oc}): 0.63 V, short-circuit current density (J_{sc}): 9.7 mA cm^{-2}, and fill factor (FF): 53.5%[27] have been reported. However, the normal device structure is not widely pursued because it implies rapid degradation of the device performance due to the use of low work function Al electrodes. It is currently a widely held opinion that such low work function metal electrodes will not contribute to the future of low cost PSCs both from a stability point of view[28] and from an economic point of view as vacuum deposition steps are uneconomic in fast low cost processing.

In the inverted device configuration, only a handful of reports that utilizes PEDOT : PSS as transparent electrode are present. The first report was made by Hau et al.[29] in which they used hcPEDOT : PSS as front electrode in two device types: one with PEDOT:PSS as back electrode and second one with Ag as back electrode. A maximum PCE of 3.08% was achieved with PEDOT : PSS as front electrode and Ag as back electrode whereas the cells showed poor rectification and photovoltaic behavior PCE: 0.47%, V_{oc}: 0.31 V, J_{sc}: 5.94 mA cm^{-2}, and FF: 27.7%) when PEDOT : PSS is used for both electrodes, The poor performance in the latter case was attributed to a high sheet resistance of hcPEDOT : PSS (>400 $\Omega\square^{-1}$) used for both electrodes and to the reduced built-in field of the device due to the symmetric PEDOT : PSS electrodes. Zhou et al. fabricated a similar semi-transparent metal free cells with a new generation hcPEDOT : PSS (115±10 $\Omega\square^{-1}$) as both electrodes.[30] The solar cells showed good rectification properties along with maximum photovoltaic properties of PCE: 1.1%, V_{oc}: 0.55V, J_{sc}: 4.4 mA cm^{-2}, and FF: 45%. Zhou et al. attributed the observed improvement in their device in comparison with Hau et al. to improved ZnO films which were deposited by Atomic Layer Deposition. Recently, Larsen-Olsen reported a PCE of 2.69% with a new generation low band gap polymer-based solar cell processed with a roll coated hcPEDOT : PSS as the front electrode in combination with PEDOT : PSS/Ag as the back electrode.[31] Such a PCE was nevertheless 40% lower to that achieved on ITO-based reference cells.

Combination of Metal and Polymers (Semi-)transparent Conductors

Despite the development of highly conductive formulations of PEDOT : PSS, its sheet resistance (10^2–10^3 $\Omega\square^{-1}$) still remains significantly higher than ITO (10–60 $\Omega\square^{-1}$) as a result of which stand-alone PEDOT : PSS front electrodes have yielded lower power conversion efficiencies than ITO-based control devices. A way to further improve upon the conductivity of PEDOT : PSS was shown by Aernouts et al. by using a combination of metal grid and PEDOT : PSS composite electrodes. Such a composite electrode when used in place of ITO in normal structure solar cells resulted in a threefold decrease in series resistance (R_s) from > 1 k Ω in cells with only PEDOT : PSS as electrode to 400 Ω for composite electrodes, ultimately resulting in a threefold increase in J_{sc}.[26] Thereafter, Glatthaar et al. investigated the composite electrode as transparent conductor in an inverted device structure where PEDOT : PSS was deposited on top of the photoactive layer and a metal was the last layer deposited by thermal evaporation in a layer sequence Al/Ti/P3HT : PCBM/PEDOT : PSS/Au grid. The differences between normal and inverted device structures are shown in Figure 3. Subsequently, several investigations followed that dealt with the optimization of grid design, deposition methods for grids, upscaling, etc. The challenge for using such a composite electrode is the optimization required between shadow losses due to the metal grids and the resistive losses due to the resistance of the combined PEDOT : PSS/metal electrode. Depending on the sheet resistance of PEDOT : PSS, completely different configurations of metal grid design are required in the optimization of the cells.[32] Overall, the surface coverage of the metal grids should be as small as possible so as to minimize loss of incoming radiation reaching the photoactive layer. Kang et al. noted that one can minimize the surface coverage but maintain the conductivity by increasing the line height.[33] In general, for a given PEDOT : PSS, the optimized geometry of the metal grid that results in minimum fractional power loss due to shadowing from the metal grids is simply given by the empirical relation ($W/W + S$) where W is the grid width and S is the grid separation.[32,34] Galagan et al. employed a one-dimensional numerical model

Applied Polymer SCIENCE

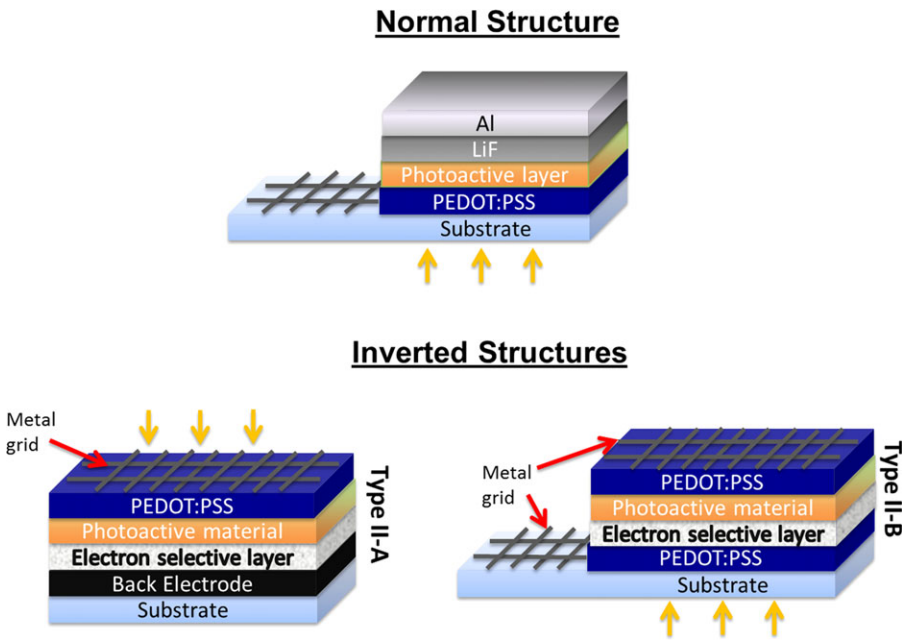

Figure 3. Normal and inverted device structure in which PEDOT : PSS/metal grids are used as transparent conductors. The arrows point to the front grid exposed to illumination.

based largely on ohm's law to predict the optimum metal grid spacing in the front electrode (PEDOT : PSS/Ag grid) resulting in maximum PCE of PSCs. Their model accounted for ohmic losses due to resistance of the metal grid lines and the PEDOT : PSS layer, and the active area loss due to shadowing from the metal grid lines. They later fabricated actual ITO-free PSCs with varying metal grid spacing and found that the PCE of actual devices corresponded well with the model predicted values.[36]

In several investigations based on laboratory scale devices, the composite metal grid and PEDOT : PSS transparent conductor layers resulted in a performance similar to ITO-based solar cells in both normal and inverted device geometries.[32,33,36] The focus after the early reports was to find up-scale compatible methods of deposition for metal grids. Some methods used for deposition of metal grids are lithography,[32,35,37] thermal evaporation through shadow masks,[38–40] sputtering in combination with photolithography for patterning,[41] microfluidic deposition and nanoimprinting methods,[33] precision weaved metalized polymer fabric electrodes,[42] and printing methods such as screen printing,[6] ink jet printing,[35,43] and flexographic printing. Among all these methods, only the printing methods are readily adoptable in fast large scale processing of low cost PSCs at this stage even if several of the other methods such as nanoimprint and lithography has been claimed as compatible with upscaling while being studied on laboratory scale devices with area as low as 0.1 $cm.^2$ They are yet to be shown on large scales.[33,39]

There are some reports on R2R production of ITO-free large area modules based on inverted structures using composite PEDOT : PSS/metal grids as the front electrode and metals (Cu and Ti; Ag; Cr/Al/Cr) as the back electrodes[44–46](Device structure Type II-A in Figure 3). Metal grids were deposited by screen printing using Ag pastes. In all these reports, poorly performing devices were obtained which was mainly ascribed to the poor transmission (<30% in the absorbing wavelength range of P3HT : PCBM) of the thick front PEDOT : PSS electrode in addition to the loss of the active area due to shadowing from the metal grid. Thick PEDOT : PSS was necessary to avoid damage of the photoactive polymer due to solvent from the metal paste diffusing to the active area. Later, it was shown that the use of UV curable Ag paste could alleviate this problem.[6] These reports further emphasized the need to find an efficient R2R compatible technique for deposition of metal grids. Galagan et al. employed screen printed metal grids in combination with highly conductive PEDOT : PSS as the front electrode in solar cells on flexible substrates (4 cm^2 area) with a normal device structure (Figure 3) and obtained superior power conversion efficiencies to equivalent ITO-based cells.[36] Such a device structure circumvented the damaging effect of solvents from screen printable inks. Figure 4 shows an image of a cell with screen printed Ag and PEDOT : PSS front electrode as studied by Galagan et al. However, such a device had low reproducibility due to topography of the metal grids that led to short circuits. A solution to this problem was to embed metal grids into the substrates as was done by Galagan et al. in the same report. Subsequently, Galagan et al. demonstrated the use of ink-jet printing as an alternative R2R compatible technique for printing of metal grids thereby avoiding the need for embedded grids on substrates.[35,43] With careful optimization of grid height facilitated by the higher resolution of ink jet printing, a PCE of 1.48% on flexible foil was achieved. Galagan et al. further demonstrated lithographically deposited Mo/Al/Mo as current collecting grids having better topology in comparison with ink-jet printed grids.[35] One recurrent result from these studies is that the use of metal grids leads to lower series resistance in solar cells which is manifested in an increased FF. ITO, on the other hand, causes increasing efficiency losses on scaling up due

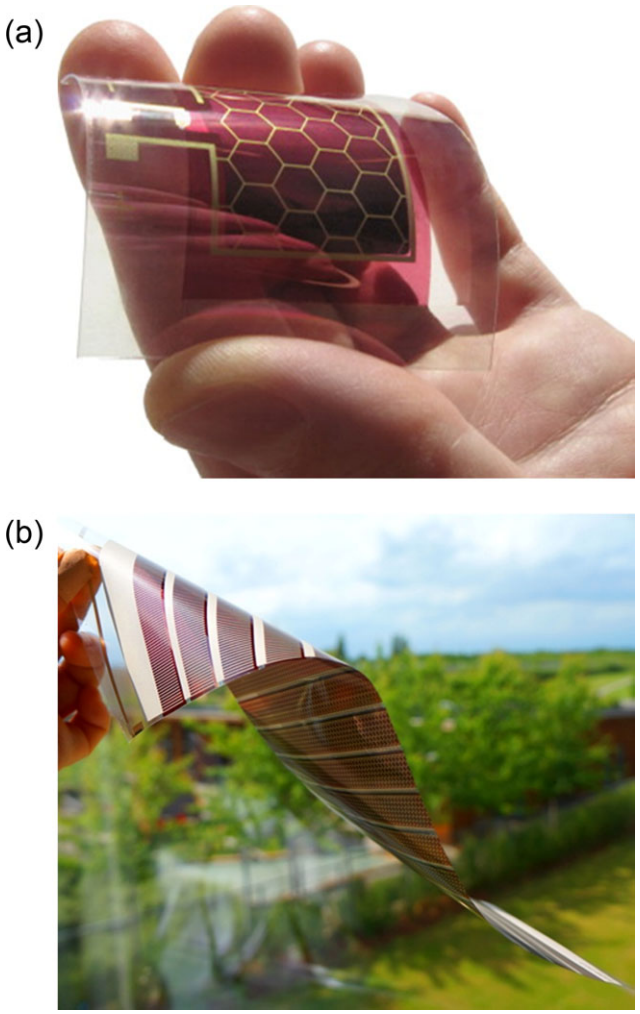

Figure 4. a) ITO-free PSC (2 × 2 cm^2) with screen printed Ag grid and highly conductive PEDOT: PSS as front electrode and evaporated Al back electrode employed in normal device structure.[37] Reprinted from Ref. [37], with permission from ©Elsevier; b) a large area highly flexible PSC modules completely processed by vacuum-free R2R printing and coating.[49]

increasing series resistance with increasing device area.[47] Such an effect is more pronounced with ITO on flexible substrates such as polyethylene terephthalate (PET) which has higher sheet resistance than ITO on glass.

Recently, Yu et al. demonstrated vacuum free all R2R processed PSCs employing high conductive PEDOT : PSS/metal grid as a front electrode and PEDOT : PSS/metal grid as the back electrode in an inverted structure.[48] Metal grids were printed by three R2R methods: R2R thermal imprinting of embedded grids, R2R ink jet printing, and R2R flexographic printing. R2R flexographic printed and R2R embedded grids delivered similar albeit unprecedented performance for fully R2R processed vacuum-free large area ITO-free cells (active area 6 cm^2) under ambient conditions with flexo grids having a PCE: 1.82%, J_{sc}: 7.1 mA cm^{-2}, V_{oc}: 5.1 V; FF: 51.2%; and embedded grids with PCE: 1.92%, J_{sc}: 7.06 mA cm^{-2}, V_{oc}: 0.50 V, FF: 54.6%. The raised topography and relatively poor conductivities in the R2R ink-jet printed silver grids resulted in significantly lower PCE due to lower FF and J_{sc} as a result of shunt paths: PCE 0.75%, J_{sc}: 4.27 mA cm^{-2},V_{oc}: 0.50 V, and FF: 35.1%. Among all these techniques, flexographic printing emerged to be the favorable low cost technique presenting no topography issues and the need for multiple R2R steps as required for thermal imprinting of embedded grids. Recently, an all R2R processed, large area, highly flexible ITO-free module with flexographic printed grids/hc PEDOT : PSS as front electrode were reported with power conversion efficiency of 1.6% on module with active area >120 cm^2 [Figure 4(b)].[49] These modules were subjected to several normal and accelerated lifetime testing conditions and were found to be rather stable under operational and storage conditions expected for ICT and mobile applications as well as for outdoor conditions.

Metals

Before the discovery and subsequent dominance of ITO as the material of choice for transparent conductors over the last four decades,[50] very thin metals usually evaporated were used as semitransparent conductors in optoelectronics. With the advent of ITO that exhibited far superior properties, these thin semitransparent metals were rapidly replaced by ITO. However, the economic and physical incompatibility of ITO in low cost applications particularly has led to revisiting metals as an ITO substitute. Ultra-thin metal layers and metal nanowires are investigated as potential ITO replacements.

Ultra-Thin Metal Layers. Surface scattering of free charge carriers in thin metal films causes an inverse relationship between film resistivity and thickness. As a result, there is a threshold below which further reduction in thickness leads to dramatic increases in sheet resistance of the metal film. Usually, the limit is between 5 and 10 nm for commonly employed electrode metals such as Al, Au and Ag.[51–53] Transmission, on the other hand, follows Beer-Lambert law with increasing thickness resulting in decreasing transmission. Hence, there is a trade-off between transmission and sheet resistance similar to the PEDOT : PSS layer as described earlier. Usually a transmission of ~60% is observed in ultra-thin metal films, for example Ag films at a thickness of 10 nm (Figure 5).[51,52]

O'Connor et al. demonstrated the use of semi-transparent thin metal electrodes in small molecule solar cells (SMSCs) and theoretically investigated the dependence of sheet resistance on the thickness of the commonly employed metals in organic solar cells: Au, Al, and Ag using Fuchs-Sondheimer (FS)-Mayadas—Shatzes (MS) model.[52] They further investigated the effect of layer thickness on J_{sc} of copper pthylocyanine: fullerence (CuPc: C_{60}) based bilayer and bulk heterojunction solar cells using optoelectronic modeling and consequently experimentally verified the modeling results. While FF and V_{oc} vary slightly within the range of thickness of the semitransparent metal explored (8–20 nm), J_{sc} was strongly dependent on thickness due to the in-coupling of light through the transparent metal conductor film. In an early report, O'Connor et al. had shown the use of an external transparent capping layer on the ultra-thin metal films can improve device performance.[54] Similar work was

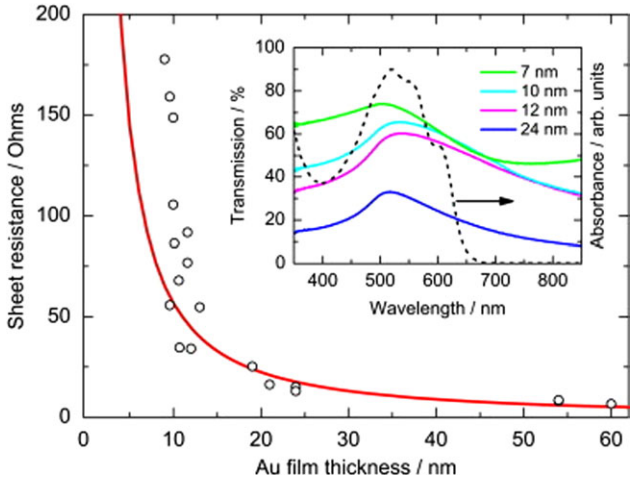

Figure 5. Thickness dependence of sheet resistance in ultra thin gold films determined by simulation based of FS-MS model (solid line) and experimentally verified (dots). Inset shows transmission of ultra-thin Au films with various thicknesses. The dashed line is absorbance of P3HT:PCBM. Reprinted from Ref. [51], with permission from ©Elsevier.

reported by Meiss et al. who used an organic capping layer in inverted solar cells.[55,56] Metals exhibit high reflection. For example, calculations have shown that while absorption of 10 nm thick silver is merely 3%, reflections can amount to 63%.[57] A capping layer can suppress this reflection and induce a desired interference pattern enhancing the amount of impinging photons on the photoactive layer in thin film solar cells. In thick film solar cells such as PSCs, however, such a phase tuning of the field maximum may result in only minute difference that do not justify the use of additional processing steps needed for application of capping layers as has been shown for optical spacers which is a similar concept to capping layers.[58]

Al-Ibrahim et al. first utilized ultra-thin metal replacement to ITO in a poly(3-hexylthiophene): [6,6]-phenyl-C_{61}-butyric acid methyl ester (P3HT : PCBM) based inverted device and compared it with an reference device with ITO as transparent conductor. The inverted device structure with Si-substrate/Ti/P3HT : PCBM/PEDOT : PSS/Au (8 nm) resulted in PCE: 1.12%; V_{oc}: 550 mV, J_{sc}: 6.25 mA cm^{-2}; FF: 33% on an active area of 0.25 cm^2.[53] Ajuria et al. presented a comprehensive report where ultra-thin gold layers were vacuum deposited as the first deposited layer (bottom electrode) or the last deposited layer (top electrode) in a ITO-free inverted device with the layer sequence Au /ZnO/P3HT : PCBM/PEDOT : PSS/Au where the counter opaque electrode was also Au layer (100 nm). The highest PCE of 2.52% was noted for devices with semitransparent bottom layer Au (5 nm)/ZnO. Such a PCE was nonetheless lower than the ITO-based reference devices (PCE: 3.53%). The lower PCE was mainly attributed to lower J_{sc} as a result of lower incoupling of light into the device. Semitransparent top electrode (PEDOT:PSS/Ag 10 nm) in ITO-free device resulted in the lowest PCE (1.75%) due to yet lower incoupling of light caused by the absorption of the PEDOT: PSS layer as compared with devices based on the less absorbing transparent bottom electrode (Au 5 nm/ZnO).[59] Wilken et al. made a comparison of PEDOT : PSS/metal grid versus PEDOT : PSS/thin metal film in identical inverted devices Al/Cr/P3HT : PCBM/PEDOT:PSS/Au. It was concluded that even with a shadowing loss of 8% metal grid/PEDOT : PSS based cells have significantly higher performance than those with PEDOT : PSS/ultra-thin film Au electrodes.[51] Unfortunately, their optimization study of sheet resistance to thickness was made on Au deposited on a glass substrate (Figure 5) with extrapolation of their effect to Au deposited on PEDOT : PSS in their actual experiment. Variations in sheet resistance at a particular thickness are mainly due to varying film morphology which in turn is affected by the type of substrate and its roughness, the surface treatment of the substrate and the deposition conditions.[52] As a result, it is unlikely that the relationship of sheet resistance and transmission of thin metal layers deposited on glass will hold true when glass is replaced by an organic substrate. Without any morphological control, it is unlikely that small amounts of Au or Ag can be deposited on PEDOT : PSS as in the case of Al-Ibrahim et al. and Wilken et al. to yield continuous films. Several authors have noticed that Ag has a tendency to coalesce when deposited on organic layers in SMSCs and have independently shown different methods to achieve continuous film formation of Ag or Au on organic layers.[60–62]

Until now, thermal evaporation was the only method for deposition of ultra-thin metal films which is highly uneconomical particularly for use in the fabrication of low cost PSCs. Recently, however, a solution processed semi-transparent Ag electrode having a sheet resistance of 5 $\Omega\square^{-1}$ and a corresponding transmission of >30% was reported. It was observed that the addition of a thin ZnO nanoparticle layer (solution-processed) leads to significant improvement in transmission. The thin film Ag/ZnO electrode was subsequently employed in fabrication of all-solution based R2R processing of large area PSC modules.[63]

Metal Nanowires. Ultra-thin metal films particularly by use of low cost printing and coating techniques for large area are unlikely to deliver a transmission and conductivity comparable to that of ITO**.** Dispersed random networks of metal nanowires (NW), on the other hand, can exhibit transmission and conductivity even superior to ITO. This was first reported by Lee et al. who pioneered the work on solution processing of metal nanowires for application in organic solar cells.[64] A random network of metal nanowires causes enhanced scattering of light resulting in improved photocurrent generation in solar cells. Their inherent roughness may also cause improved donor: acceptor interface. Lee et al. used solution processed metal nanowires on flexible substrates as front electrode in SMSCs and found similar performance to ITO-based equivalent cells (Figure 6). However, subsequent work on normal devices was not as successful mainly because of processing challenges. For example, Yang et al. used a laminated metal nanowire electrode in normal device geometry devices and found a performance that was consistently lower than ITO-based reference cells.[66] This was attributed to lower work function difference between the AgNW/PEDOT : PSS and Al than between ITO and Al counter electrodes as employed in the reference cells. This led to lower V_{oc} in AgNW-based devices than the ITO-based reference devices. Such

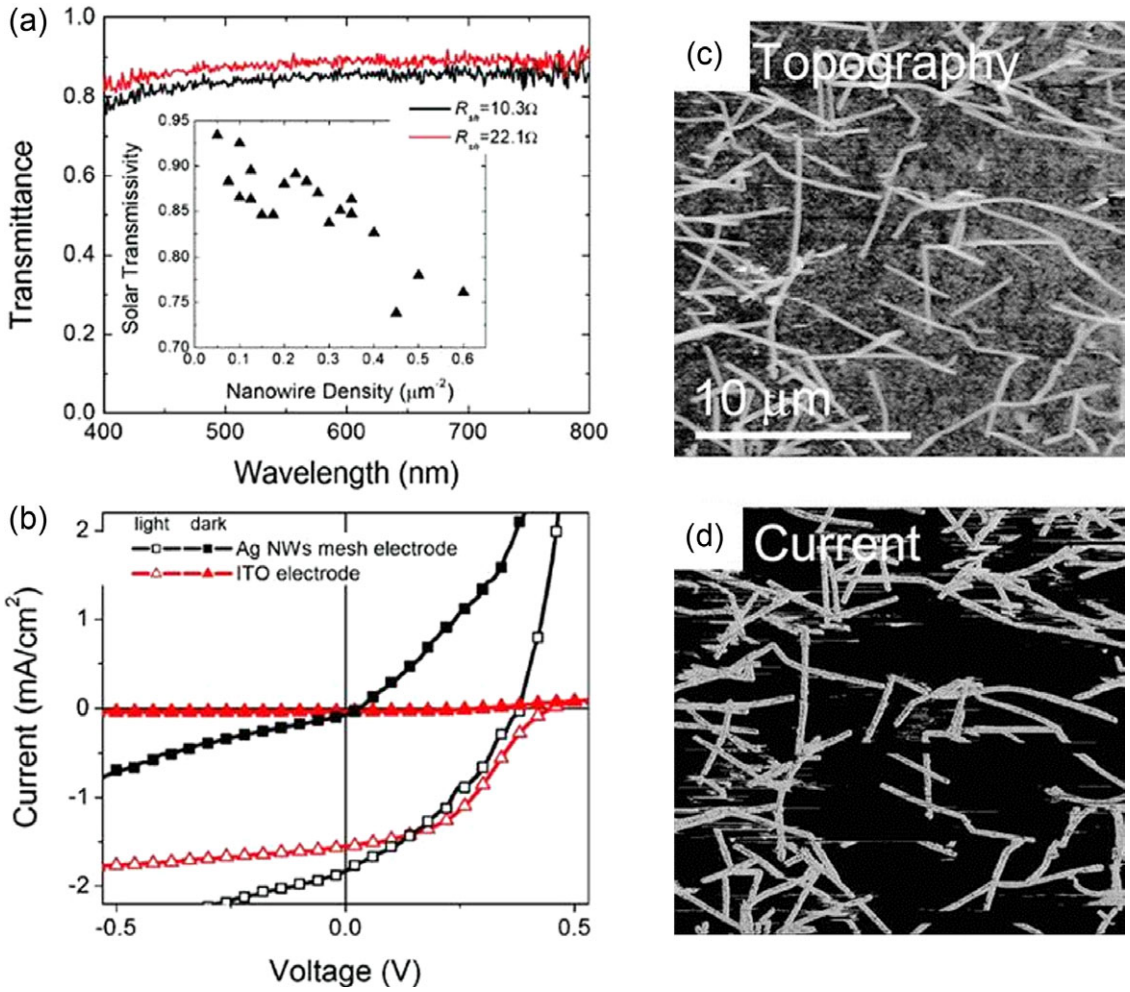

Figure 6. a) Diffuse optical transmission of silver nanowire transparent conductor with two different R_{sh} 10.3 and 22.1 $\Omega\square^{-1}$ with inset showing solar photon flux-weighted transmissivity as a function of NW density; b) JV characteristics of SMCs at 65 mW cm^{-2} at AM1.5 illumination. Reprinted from Ref. [64], with permission from ©American Chemical Society. c) Topographic AFM image (top) and current mapping of same section as topography image with current-AFM. Reprinted from Ref. [65], with permission from ©American Chemical Society.

a problem can be circumvented by tuning the work-function of the electrodes with the use of buffer layers. For example, Gaynor et al. made use of Cs_2CO_3 to alter the work function of metal back electrodes so as to maintain an appropriate work-function difference between the laminated AgNW front electrode and Ag back electrode in a P3HT: PCBM-based inverted structure and obtained a PCE of 2.5%.[67] Similarly, Leem et al. demonstrated the use of an optically transparent TiO_2 as a buffer layer on top of AgNW layers in inverted solar cells and observed a similar performance to that of ITO-based reference cells with a PCE of 3.45%.[68] Apart from tuning the work function of the electrode, such a buffer layer provide planarization of the surface roughness of the electrode, thus suppressing the formation of shunt paths. Similarly, ZnO was used as a buffer layer in inverted solar cells with AgNW front electrode by Ajuria et al.[69] and Morgenstern et al.[70] In both reports, the PCE obtained on the ITO-free AgNW devices were higher or similar to the PCE of their respective ITO-based reference cells. It was noted by Ajuria et al. that the void between individual AgNW in the film are responsible for limiting the conductivity and the charge extraction properties of the AgNW electrode particularly when the size of the void is greater than the charge carrier diffusion length. Filling up such void with a highly conductive ZnO leads to a quasi-continuous film formation bridging the void and thus suppressing charge recombination, ultimately leading to improved PCE. Ajuria et al. reported a PCE of 3.85% on glass and 3.19% on PET with AgNW/ZnO front electrode while ITO-based cells with ZnO buffer layer showed a PCE of 3.53%. Metal nanowires deposited on flexible substrates can withstand far greater flexing as compared with ITO. De et al. have shown a silver nanowire film with 75% transparency and a sheet resistance of 3.4 $\Omega\square^{-1}$ at a nanowire density of 70 mg m^{-2}. Such a film albeit at a slightly higher nanowire density of 79 mg m^{-2} could withstand 1000 bend cycles without any change in sheet resistance whereas an ITO substrate catastrophically failed after a 160 bend cycles.[71]

The few reports have successfully demonstrated the potential of AgNW network films as serious contenders in the race to

Applied Polymer SCIENCE

replace ITO. Currently, research on metal nanowires is slowly being directed towards finding large scale compatible processing techniques.[72–74] The early reports have also identified several challenges that remain to be solved, for example, the poor adhesion of the nanowires on substrates;[71] their rough topology that leads to shunt paths in the solar cells when used as either the first or last deposited electrode;[64,67] the use of surfactants for dispersion of nanowires require their subsequent elimination at higher temperature than common substrates such as PET or PEN can withstand.[71] Research on AgNW films is still in its infancy and it is likely that these pressing processing issues will be solved in the near future; however the question still remains if AgNW are a cost-effective alternative to ITO. Silver has similar abundance to indium and one could argue that if we have an indium problem, then we also have a silver problem.

Carbon Nanotubes and Graphene

Carbon Nanotubes. Not too long after the first report on carbon nanotubes in 1991 by IIjima that the excellent mechanical and electrical properties of carbon nanotubes were identified. Single wall carbon nanotubes (SWCNTs) have a current conductivity of 1 to 3 $\times$ 10^6 S/m and mobility of 100,000 cm^2 V^{-1} s^{-1}.[75,76] However, a random network of CNTs in films have the highest reported conductivity of 6600 S cm^{-1} and mobilities in the 1 to 10 cm^2 V^{-2} range as a result of large junction (surface to surface) resistance.[75] A wide set of advanced applications have been envisioned for CNTs but their commercial use has been hindered by several processing issues. Such processing issues, particularly purification of CNTs and their dispersion, have proven to be major challenges. Bulk CNTs comprises a mixture of semiconducting (1/3) and metallic (2/3) forms causing non-ohmic contacts in films. In addition, their high surface energy renders them very susceptible to bundling. Although CNTs can be dispersed in various solvents using different dispersing agents such as surfactants, they tend to re-bundle once the dispersing agents are removed. A common method of deposition of CNTs involves: dispersion in a solvent with the use of dispersing agents, vacuum filtration, removal of surfactants by repeated washing of the filtrate CNTs, and finally transferring the CNT filtrate to a substrate of choice with the use of e.g. a (patterned or un patterned) polydimethylsiloxane (PDMS) stamp. Such a transfer method was employed first by Zhou et al. to deposit SWCNTs on PET achieving a sheet resistance of 120 $\Omega\square^{-1}$ with a transmission similar to ITO in the visible region.[77] Several in-depth reviews on CNT properties and processing, and their varied applications in solar energy conversion can be found elsewhere.[75,78-80]

CNTs as a potential transparent conductor was identified by Lee et al. when they used a 1000 Å thin SWCNT film with a 60% transmission as a transparent p-contact in GaN LED.[81] It was, however, Wu et al. who is given credit for highlighting the potential of SWCNTs as transparent conductors. For a 50 nm thin film of p-doped SWNT film, a sheet resistance of 30 $\Omega\square^{-1}$ with a transmission of >70% over visible region of the light spectrum was reported.[82] Such properties of SWCNT films have set a benchmark as subsequent reports have been mostly unable to achieve similar results (see Table I). A large number of parameters (largely uncontrollable) affect CNT conductivity

Table I. Compilation of Selected Few Results of Properties of Carbon Nanotube-Based Transparent Conductors and the Photovoltaic Parameters of their Corresponding Organic Solar Cells

Device	Treatment of SWCNT	Active area (mm^2)	R_s of graphene film ($\Omega\square^{-1}$)	Transmittance (%)	J_{sc} (mA $cm^{[minus]2}$)	V_{oc} (V)	FF (%)	PCE (%)	Refs.
Glass/SWCNT/PEDOT : PSS/P3HT:PCBM/Ga : In	None	7	282	85 (650 nm)	6.65	0.5	30	0.99	83
PET/SWCNT/PEDOT : PSS/P3HT:PCBM/Al	Surfactant	4	200	NA	7.8	0.61	52	2.5	84
Glass/SWCNT/PEDOT : PSS/P3HT:PCBM/Al	Acid	10	50	70 (650 nm)	9.2	0.56	29	1.50	85
Glass/MWCNT mat/PEDOT : PSS/	NA	9	588	50	5.5	0.49	49	1.32	86
Glass/SWCNT/PEDOT : PSS/P3HT:PCBM/Ca/Al	Cellulose + acid	3	60	70 (400–1800 nm)	11.5	0.58	48	3.1	87
Glass/SWCNT/P3HT : PCBM/Ca/Al	Cellouse + acid	NA	24	NA	11.4	0.54	55.4	3.37	88
Glass/SWCNT/P3HT : PCBM/LiF/Al	Acid	NA	51	69	11.1	0.59	54.2	3.6	89

such as purity, lattice perfection, bundle size, wall number, metal/semiconductor ratio, diameter, length, and doping level which vary among studies. Tenent et al. reported a sheet resistance of 60 $\Omega\square^{-1}$ for a 40 nm thick film using less defect prone SWCNTs that are grown using laser vaporization and are p-doped.[87] Note that sheet resistance of CNT films is dominated by junction resistance and the use of doping by acid treatments have been shown to cause a threefold decrease in junction resistance and a 30% increase in the nanotube conductivity when compared with pristine untreated samples[90] (Figure 7). So far, spray deposition is the most up-scalable low cost technique reported for fabrication of SWCNT transparent conductors. Using this method, Tenent et al. reported a sheet resistance of 110 $\Omega\square^{-1}$ (pristine SWCNT) and 37 $\Omega\square^{-1}$ (doped SWCNT) with transmission of 78 and 76% (550 nm) respectively (Figure 7).[87] The large spread in the properties of SWCNT films (Table I) is indicative of the processing and purification challenges that continue to delay the advancement of SWCNT transparent conductors from proof-of-principle to actual applications.

Apart from processing challenges, the roughness of the CNTs thin films and their adhesion to the substrates has been equally impeding factors for the efficacy in organic solar cells. Shunts due to roughness of the SWCNT surface is circumvented by using 0.5 to 1 μm thick active layer[83,85] which ultimately undermined the efficiency of these devices. PEDOT: PSS was used as a planarization layer and a three-fold increase in device performance was observed.[85] Rowell et al. showed significant improvement in roughness (10 nm over 25 μm^2 scan area) using a PDMS based transferring method for surfactant assisted dispersion of un-doped SWCNTs. The film had a transmission of 85% and a sheet resistance of 200 $\Omega\square^{-1}$.[84] Ultimately, the improved film properties were reflected in the PSCs (PCE: 2.5%) which was comparable to ITO-based reference devices (PCE: 3%).

Apart from SWCNTs, multiwalled carbon nanotube (MWCNT) sheets or mats were incorporated in PSCs[86,91] soon after their simple processing possibility was demonstrated.[92] These sheets were strong, highly transparent, and conductive. However, the rough topology required planarization with PEDOT : PSS ultimately resulting in a 50% light transmission to the photoactive layer. Nevertheless, a PCE of 1.32% was achieved in a normal device structure.[86]

All the earlier reported devices have an active area of <1 cm^2 of area and used thin film fabrication techniques that are not readily scalable. In regard to processing of large area CNT thin films, progress has been slow and so far spraying techniques are the most scalable technique investigated.[87,88,93] Tenent et al. dispersed SWCNTs in aqueous solvents with high molecular weight (~90,000 MW) cellulose (sodium carboxymethylcellulose, CMC) as dispersing agent.[87] With the use of ultrasonic spraying, the CMC-based dispersion is deposited over large areas (6 × 6 inches) (Figure 7). Finally, the film is exposed to nitric acid to remove CMC while simultaneously functionalizing or doping the nanotubes. Such a film is found to be highly homogenous (rms roughness of 3 nm scanned over 100 μm^2 area) with superior electrical conductivity and optical transmission and resulted in PCE of 3.1% in PSCs, albeit slightly lower than ITO-based reference devices (PCE: 3.6%). Later, the same group avoided the use of PEDOT : PSS as planarization and hole transport layer and instead used 900 nm thick active layer and observed a PCE of 3.7%. The SWCNT film had a sheet resistance of 30 $\Omega\square^{-1}$.[88] It was hence concluded that SWCNTs can replace both ITO and hole transport PEDOT : PSS buffer layers and that these devices show much higher J_{sc} as a result of higher transmission beyond the visible region (above theoretical predictions of J_{sc} based on visible transmission) (Figure 7). Similarly, Kim et al. reported similar SWCNTs deposition technique to Tennent et al. with the difference that surfactants are used instead of CMC and deposition is done by pressure driven spray coating. Kim et al. evaluated the effect of several surfactants[94] and compared patterning of large area through lithography and contact stencil.[89] The dip-coating of bare substrate in 1% solution of 3-aminopropyltriethoxy silane in deionized water is found to improve adhesion of SWCNTs onto the substrates due to the formation of cross-linked siloxane on the surface of substrates. The final optimized device had a sheet resistance 51 $\Omega\square^{-1}$ with a transmission of 69% (at 550 nm) and resulted in PSCs with PCEs of 3.6% and 2.6%, respectively on glass and PET substrates. This is the highest reported performance of PSCs with SWCNTs transparent conductors.

From all aforementioned reports that incorporated SWCNT-based transparent conductors in PSCs, two issues clearly emerge: firstly, nearly all devices are studied in a normal geometry and secondly, the processing choices are very limited for large area substrates. Spray coating seems to be the only technique that allows for easy processing on large area substrates. There is a long way before SWCNTs transparent conductors can their make way into R2R processing. The proof-of principle has been demonstrated and the task ahead needs to show its flexibility and feasibility with inverted devices and performance with respect to PSCs stability if any. For example, Tenent et al. observed an increase in sheet resistance of spray coated films from 150 to 240 $\Omega\square^{-1}$ over a 10-day period.[87] Such effects are deteriorating for PSCs and require further investigations.

Graphene. The metamorphosis of graphene from the theoretical world to physical reality in 2004 has presented the possibility of a number of advanced applications: transparent conductors being one of them. With less than 0.1% reflectance and 2.3% absorbance for every single graphene sheet, the theoretical transmission limit of a single layer graphene sheet is 97.7% and the corresponding sheet resistance for undoped graphene sheet is 6 $k\Omega\square^{-1}$.[95,96] A higher value of transmission (99%) and lower sheet resistance (30 $\Omega\square^{-1}$) than the theoretically predicted values have been reported in experimental results and are attributed to the presence of defects, increasing stacking of graphene sheets, and extrinsic doping[97,98] Sheet resistance of graphene decreases rapidly with increasing stacking of graphene sheets and with doping, however, at the expense of optical transmission. In the case of sheet resistance of 30 $\Omega\square^{-1}$, the corresponding transmission was 90% which is nonetheless comparable to ITO. Apart from sheet resistance and transmission, several other properties such as the high chemical and thermal stability, high charge carrier mobility (200 $cm^2\ V^{-1}\ s^{-1}$), high current carrying capacity

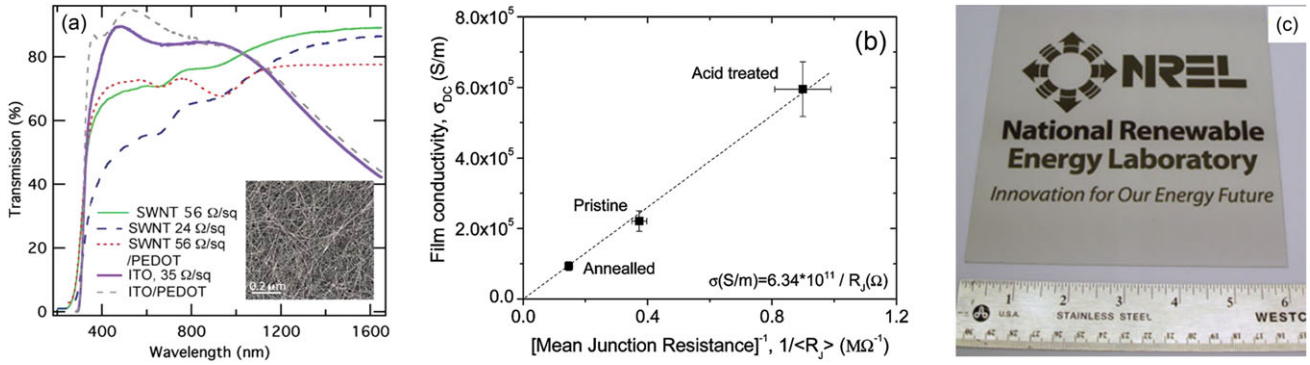

Figure 7. a) Comparison of transmission spectra for ITO and SWCNT (with and without PEDOT : PSS). Inset shows TEM image of ultrasonically sprayed films; b) Plot of measured film conductivity as a function of the inverse of mean junction resistance; c) Ultrasonically spray deposited large area (6 × 6 inch^2) SWCNTs film.[87] Reprint permissions: (a and b) Reprinted from Refs. 88 and 90, with permission from ©American Institute of Physics. c) Reprinted from Ref. [87], with permission from ©John Wiley and Sons.

(3×10^8 A cm^{-2}), high stretchability, and low contact resistance with organic materials renders graphene a very favourable alternative to ITO.[99,100] Translating theoretical wonders of graphene into real applications has been met with several challenges.

The processing of high quality graphene remains the biggest challenge. High quality graphene is either micromechanically cleaved or grown by chemical vapor deposition; both of which are not low cost and large scale compatible. In principle, a monolayer of graphene possesses ballistic charge transport due to delocalization of electrons over the complete sheet, however, in practice defects are introduced during growth and processing of graphene. Such defects, for example, lattice defects, grain boundaries, and oxidative traps due to functionalization results in high sheet resistance of graphene.[95,101] As a result, graphene films must be made thicker than a monolayer to attain practical sheet resistance. Defects are more prominent in graphene films processed by solution based methods such as liquid phase cleaving with ultra-sonication or by reduction of graphene oxide. Although these techniques provide lower cost alternatives to processing of graphene, however, graphene produced by such methods exhibit poor properties with sheet resistance in the kΩ□$^{-1}$ range due to structural defects and poor interlayer contact as a result of vigorous exfoliation and reduction processes.[102] Several reviews on the properties and processing of graphene are present elsewhere[97,100,103] and a recent review elaborates on the application of graphene as electrodes in electrical and optical devices.[104] Henceforth, we briefly present the use of graphene as transparent conductors in organic solar cells.

At this infant stage, it is difficult to estimate when research on graphene as transparent conductor will bear fruit. The difficulties in low cost high quality production of graphene and the very few proof-of-concept studies on utilizing graphene as transparent conductors in organic solar cells (yet fewer in PSCs) highlights the need for more research emphasis on processing. The earlier reports on graphene as transparent conductors were adopted in dye sensitized and small molecule solar cells, however, the performance of such devices were limited (PCEs of <1%) by the high sheet resistance of the films which is often in the kΩ range.[101,105] Although it has been demonstrated that fabrication of large area (30 inch) CVD graphene on Cu substrates can give a sheet resistance as low as 30 Ω□$^{-1}$ with 90% transmission,[98] it appears that reproducing such results has not been possible in independent laboratories. De Arco et al. demonstrated the achievement of CVD graphene with a transmission of 72% (550 nm) and a sheet resistance of 230 Ω□$^{-1}$ but employed an optimized graphene with 3.5 k Ω□$^{-1}$ with 89% transmission to successfully demonstrate a small molecule solar cell with PCE of 1.18%.[106] Graphene is hydrophobic and requires functionalization (e.g. UV/ozone treatment) to improve its wetting properties. Such functionalization creates defects in graphene sheets increasing its sheet resistance and therefore limiting the final performance. Noncovalent functionalization improves wetting while maintaining the structural integrity of graphene. Such a noncovalent functionalization of graphene with self-assembled pyrene butanoic acid succidymidyl ester (PBASE) improved its wetting properties towards PEDOT:PSS and resulted in a greater than two-fold increase in PCE.[107] By depositing a 20 Å thin layer of MoO_3 over graphene, Wang et al. demonstrated improved wetting properties of graphene toward PEDOT : PSS as well as improved work function of graphene electrodes.[108] Their best device with the structure: doped-graphene/MoO_3/PEDOT : PSS/P3HT : PCBM/LiF/Al resulted in a PCE of 2.5% which was 83.3% of the PCE obtained on ITO-based equivalent devices (3%). They further noted that the use of MoO_3 results in superior results than the use of PBASE (PCE of 2%) for surface functionalization graphene to improve its hydrophilicity. The main contribution of this report was however in processing of graphene using a simplified PMMA-based transfer method through which they were able to produce multiple layers of graphene with the best results found with four layer graphene exhibiting a sheet resistance of 80 Ω□$^{-1}$ and a transmission of 90% (550 nm). The doping of graphene with $AuCl_3$ is reported to reduce sheet resistance of graphene by 77% with only 2% decrease in transmission.[109] Park et al. noted an improvement in PCE from 1.36% for undoped graphene to 1.63% for $AuCl_3$-doped graphene film.[110] Choe et al. used high quality CVD grown multilayer graphene films (15 layers) to make P3HT:PCBM-based PSCs and obtained a PCE of 2.60% with the use of TiO_2 electron selective buffer layer and graphene grown at 1000°C. A strong

Table II. Compilation of Selected Few Results of Properties of Graphene-Based Transparent Conductors and the Photovoltaic Parameters of their Corresponding Organic Solar Cells

Structure	Area (mm^2)	R_{sh} ($\Omega\square^{-1}$)	T (%)	J_{sc} (mA cm^{-2})	V_{oc} (V)	FF (%)	PCE (%)	Refs.
Quartz/graphene/CuPc/C_{60}/BCP/Ag	0.81	5×10^3 -1 $\times 10^6$	85-95	2.1	0.48	34	0.4	101
PET/CVD-graphene/PEDOT : PSS/CuPc/BCP/Al	0.7	3.5×10^3	89	4.73	0.48	52	1.18	106
Glass/CVD graphene: PBASE/PEDOT : PSS/P3HT : PCBM/LiF/Al	n.a.	1350-210	91-72	6.05	0.55	51.3	1.71	107
Glass/graphene/MoO_3/PEDOT : PSS/P3HT : PCBM/LiF/Al	n.a	80	90	8.5	0.59	0.51	2.5	108
Glass/graphene/PEDOT : PSS/P3HT : PCBM/TiO_2/Al	n.a.	610 ± 140	86.9 ± 1.2	9.03	0.60	48	2.60	111
Quartz/$AlCl_3$-doped graphene/PEDOT : PSS/CuPc/C_{60}/BCP/Ag	1.21	300-500	91.2-97.1	9.15	0.43	42	1.63	110

R_{sh} is sheet resistance and T is transmission.

dependence of device performance on the growth temperature of graphene was found.[111]

As apparent from Table II, almost all organic solar cells studied with graphene as transparent electrode serves the objective of proof-of-concept. Sheet resistance is seldom lower than 200 $\Omega\square^{-1}$ which may not be critical in small area devices but will prove detrimental to photovoltaic properties upon upscaling. For graphene to be a meaningful replacement to ITO, sheet resistance has to be significantly reduced with processing conditions conducive to low-cost fabrication. At this juncture, graphene represent a long term possibility.

ITO-FREE PSC MODULE APPLICATION/DEMONSTRATION

There has been only one example of an application of ITO-free OPV. The solar cell technology known as *IOne*[112] represents true progress when compared to the ITO-based *ProcessOne*[114] that has been the work horse within R2R processed OPV modules for many years. *ProcessOne* was the first truly scalable ITO-based and fully R2R processed OPV technology that has been prepared in excess of 2000 m^2 at DTU and has been used in numerous demonstrations of the technology.[114–116] It is also commercially available today from Mekoprint A/S, Denmark. *IOne* is a lower cost and significantly faster process that present no disadvantages when compared to *ProcessOne* while being both vacuum and ITO free and presenting a much better operational stability and a significantly lower materials and overall cost. The enabling feature is the *in situ* formation of a rectifying layer through a fast switching mechanism that was demonstrated to be fully R2R compatible and subsequently mass produced and product integrated in laser pointers.[117] The modules had 16 serially connected cells with the structure Ag-grid/PEDOT:PSS/ZnO/P3HT : PCBM/PEDOT:PSS. All layers were R2R processed using R2R ink jet printing for Ag grid, R2R rotary screen printing for PEDOT : PSS layers, and R2R slot die coating for ZnO and P3HT:PCBM. The cells were interconnected using a silver paste in rotary screen printing. The modules had an active area of 15.4 cm^2 and a power conversion efficiency of ~2% (Figure 8). This is the first demonstration of ITO-free polymer solar cell modules in real applications. Finally it should be noted that the *IOne* process[112] has been demonstrated in a silver free version based only on carbon with the same performance thus demonstrating that neither indium nor silver is required to make efficient and scalable OPV. The

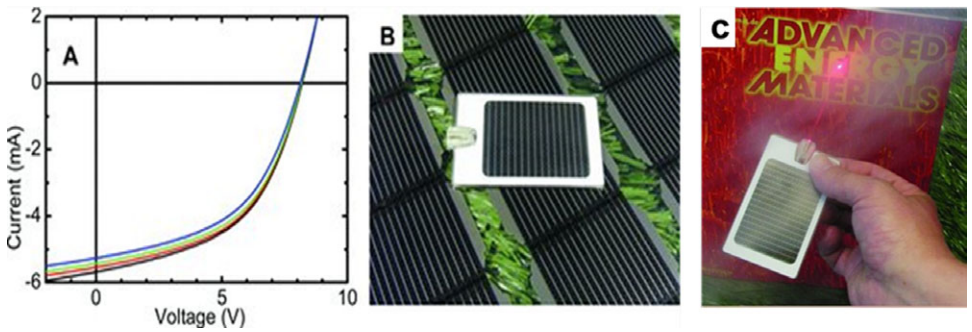

Figure 8. IV-graph for all R2R processed ITO-free PSC modules complete modules (a) incorporated in demonstrator laser power pointer (b, c) (the background in b shows as printed (R2R) modules on flexible foil unwounded from a roll. Reprinted from Ref. 117, with permission from ©John Wiley and Sons.

efficient replacement of silver was achieved with carbon paste which presents superior printing and stability performance over printed silver conductors while requiring somewhat thicker printed layers to achieve the same conductivity.

CONCLUSION

Polymer solar cells present an attractive technology by the sole virtue of its low cost processing potential. It is clear that indium tin oxide cannot deliver competencies with respect regard to low cost and flexibility. Finding an alternative is crucial for the successful commercialization of PSCs. Ideally, the most compatible alternative to ITO should be solution-based and processable at temperatures compatible to common flexible substrates such as PET. While most of the alternatives presented in this review have the potential to fulfill such requirements, processing issues have impeded their progress from laboratory to large scale production. CNTs, graphene, and metal nanowires have shown remarkable properties that even surpass the benchmark that ITO has set. With the rapid progress in processing of CNT, graphene, and nanowires being reported, it is not too long before they are commercially utilized as transparent conductors for all optoelectronics in general and organic solar cells in particular. Meanwhile, the composite PEDOT:PSS/metal grid electrode remains the readily available and up-scalable alternative to ITO. Nonetheless, the most recent trend has been to replace both indium and metals such as silver through use of carbon paste and it is now clear that future of OPV is not shared with indium or silver unless they can be recycled with very high efficiency.

This work has been supported by the European Commission as part of Framework 7 ICT 2009 collaborative project HIFLEX (Grant no. 248678). The authors thank Markus Hösel and Jon Eggert Carlé and for their help with graphics and image processing.

REFERENCES

1. Xue, J. *Polym. Rev.* **2010**, *50*, 411.
2. U.S. Geological Survey (USGS). Information downloaded from: http://minerals.usgs.gov/minerals/pubs/commodity/indium/mcs-2012-indiu.pdf. Acquired on November 12, **2012**.
3. Espinosa, N.; Garcìa-Valverde, R.; Urbina, A.; Krebs, F. C. *Sol. Energy Mater. Sol. Cells* **2011**, *95*, 1293.
4. Emmott, C. J. M.; Urbina, A.; Nelson, J. *Sol. Energy Mater. Sol. Cells* **2012**, *97*, 14.
5. Azzopardi, B.; Emmott, C. J. M.; Urbina, A.; Krebs, F. C.; Mutale, J.; Nelson, J. *Energy Environ. Sci.* **2011**, *4*, 3741.
6. Krebs, F. C.; Tromholt, T.; Jørgensen, M. *Nanoscale* **2010**, *2*, 873.
7. Espinosa, N.; Hösel, M.; Angmo, D.; Krebs, F. C. *Energy Environ. Sci.* **2012**, *1*, 5117.
8. Na, S.; Kim, S.; Jo, J.; Kim, D. *Adv. Mater.* **2008**, *20*, 4061.
9. Chang, Y.; Wang, L.; Su, W. *Org. Electron.* **2008**, *9*, 968.
10. Dam, H. F.; Krebs, F. C. *Sol. Energy Mater. Sol. Cells* **2010**, *97*, 191.
11. Krebs, F. C. *Sol. Energy Mater. Sol. Cells* **2009**, *93*, 394.
12. Søndergaard, R.; Hösel, M.; Angmo, D.; Larsen-Olsen, T. T.; Krebs, F. C. *Mater. Today* **2012**, *15*, 36.
13. Kirchmeyer, S.; Reuter, K. J. *Mater. Chem.* **2005**, *15*, 2077.
14. Levermore, P. A.; Chen, L.; Wang, X.; Das, R.; Bradley, D. D. C. *Adv. Mater.* **2007**, *19*, 2379.
15. Zhang, X. G.; Butler, W. H. *Phys. Rev. B* **1995**, *51*, 10085.
16. Ha, Y. H.; Nikolov, N.; Pollack, S. K.; Mastrangelo, J.; Martin, B. D.; Shashidhar, R. *Adv. Funct. Mater.* **2004**, *14*, 615.
17. Winther-Jensen, B.; Krebs, F. C. *Sol. Energy Mater. Sol. Cells* **2006**, *90*, 123.
18. Groenendaal, B. L.; Jonas, F.; Freitag, D.; Pielartzik, H.; Reynolds, J. R. *Adv. Mater.* **2000**, *12*, 481.
19. Hsiao, Y.; Whang, W.; Chen, C.; Chen, Y. *J. Mater. Chem.* **2008**, *18*, 5948.
20. Ouyang, B. Y.; Chi, C. W.; Chen, F. C.; Xi, Q. F.; Yang, Y. *Adv. Funct. Mater.* **2005**, *15*, 203.
21. Zhang, F. L.; Johansson, M.; Andersson, M. R.; Hummelen, J. C.; Inganäs, O. *Adv. Mater.* **2002**, *14*, 662.
22. Admassie, S.; Zhang, F. L.; Manoj, A. G.; Svensson, M.; Andersson, M. R.; Inganäs, O. *Sol. Energy Mater. Sol. Cells* **2006**, *90*, 133.
23. Ahlswede, E.; Hanisch, J.; Powalla, M. *Appl. Phys. Lett.* **2007**, *90*, 163504.
24. Do, H.; Reinhard, M.; Vogeler, H.; Puetz, A.; Klein, M. F. G.; Schabel, W.; Colsmann, A.; Lemmer, U. *Thin Solid Films* **2009**, *517*, 5900.
25. Huang, T.; Huang, C.; Su, Y.; Chen, Y.; Fang, J.; Wen, T. *J. Vac. Sci. Technol. B* **2010**, *28*, 702.
26. Aernouts, T.; Vanlaeke, P.; Geens, W.; Poortmans, J.; Heremans, P.; Borghs, S.; Mertens, R.; Andriessen, R.; Leenders, L. *Thin Solid Films* **2004**, *451*, 22.
27. Na, S.; Kim, S.; Jo, J.; Kim, D. *Adv. Mater.* **2008**, *20*, 4061.
28. Jørgensen, M.; Norrman, K.; Krebs, F. C. *Sol. Energy Mater. Sol. Cells* **2008**, *92*, 686.
29. Hau, S. K.; Yip, H.; Zou, J.; Jen, A. K. *Org. Electron.* **2009**, *10*, 1401.
30. Zhou, Y.; Cheun, H.; Choi, S.; Potscavage, W. J., Jr.; Fuentes-Hernandez, C.; Kippelen, B. *Appl. Phys. Lett.* **2010**, *97*, 153304.
31. Larsen-Olsen, T. T.; Machui, F.; Lechene, B.; Berny, S.; Angmo, D.; Søndergaard, R.; Blouin, N.; Mitchell, W.; Tierney, S.; Cull, T.; Tiwana, P.; Meyer, F.; Carrasco-Orozco, M.; Scheel, A.; Lövenich, W.; de Bettignies, R.; Brabec, C. J.; Krebs, F. C. *Adv. Energy Mater.* **2012**, *2*, 1091.
32. Tvingstedt, K.; Inganäs, O. *Adv. Mater.* **2007**, *19*, 2893.
33. Kang, M.; Kim, M.; Kim, J.; Guo, L. J. *Adv. Mater.* **2008**, *20*, 4408.
34. Cheknane, A. *Progr. Photovoltaics* **2011**, *19*, 155.
35. Galagan, Y.; Zimmermann, B.; Coenen, E. W. C.; Jørgensen, M.; Tanenbaum, D. M.; Krebs, F. C.; Gorter, H.; Sabik, S.; Slooff, L. H.; Veenstra, S. C.; Kroon, J. M.; Andriessen, R. *Adv. Energy Mater.* **2012**, *2*, 103.

36. Galagan, Y.; Rubingh, J. J. M.; Andriessen, R.; Fan, C.; Blom, P. W. M.; Veenstra, S. C.; Kroon, J. M. *Sol. Energy Mater. Sol. Cells* **2011**, *95*, 1339.
37. Zou, J.; Yip, H.; Hau, S. K.; Jen, A. K. *Appl. Phys. Lett.* **2010**, *96*, 203301.
38. Zimmermann, B.; Glatthaar, M.; Niggemann, M.; Riede, M. K.; Hinsch, A.; Gombert, A. *Sol. Energy Mater. Sol. Cells* **2007**, *91*, 374.
39. Glatthaar, M.; Niggemann, M.; Zimmermann, B.; Lewer, P.; Riede, M.; Hinsch, A.; Luther, J. *Thin Solid Films* **2005**,491.
40. Zimmermann, B.; Schleiermacher, H. F.; Niggemann, M.; Wuerfel, U. *Sol. Energy Mater. Sol. Cells* **2011**, *95*, 1587.
41. Choi, S.; Potscavage, W. J., Jr.; Kippelen, B. *Opt. Express* **2010**, *18*, A458.
42. Kylberg, W.; de Castro, F. A.; Chabrecek, P.; Sonderegger, U.; Chu, B. T.; Nüesch, F.; Hany, R. *Adv. Mater.* **2011**, *23*, 1015.
43. Galagan, Y.; Coenen, E. W. C.; Sabik, S.; Gorter, H. H.; Barink, M.; Veenstra, S. C.; Kroon, J. M.; Andriessen, R.; Blom, P. W. M. *Sol. Energy Mater. Sol. Cells* **2012**, *104*, 32.
44. Krebs, F. C. *Org. Electron.* **2009**, *10*, 761.
45. Manceau, M.; Angmo, D.; Jørgensen, M.; Krebs, F. C. *Org. Electron.* **2011**, *12*, 566.
46. Krebs, F. C. *Sol. Energy Mater. Sol. Cells* **2009**, *93*, 1636.
47. Lungenschmied, C.; Dennler, G.; Neugebauer, H.; Sariciftci, S. N.; Glatthaar, M.; Meyer, T.; Meyer, A. *Sol. Energy Mater. Sol. Cells* **2007**, *91*, 379.
48. Yu, J.; Kim, I.; Kim, J.; Jo, J.; Larsen-Olsen, T. T.; Søndergaard, R. R.; Hösel, M.; Angmo, D.; Jørgensen, M.; Krebs, F. C. *Nanoscale* **2012**, *4*, 6032.
49. Angmo, D.; Gevorgyan, S. A.; Larsen-Olsen, T. T.; Søndergaard, R.; Hösel, M.; Jørgensen, M.; Gupta, R.; Kulkarni, G. U.; Krebs, F. C. *Org. Electron.*, submitted.
50. Kumar, A.; Zhou, C. *ACS Nano* **2010**, *4*, 11.
51. Wilken, S.; Hoffmann, T.; von Hauff, E.; Borchert, H.; Parisi, J. *Sol. Energy Mater. Sol. Cells* **2012**, *96*, 141.
52. O'Connor, B.; Haughn, C.; An, K.; Pipe, K. P.; Shtein, M. *Appl. Phys. Lett.* **2008**, *93*, 223304.
53. Al-Ibrahim, M.; Sensfuss, S.; Uziel, J.; Ecke, G.; Ambacher, O. *Sol. Energy Mater. Sol. Cells* **2005**, *85*, 277.
54. O'Connor, B.; An, K. H.; Pipe, K. P.; Zhao, Y.; Shtein, M. *Appl. Phys. Lett.* **2006**, *89*, 233502.
55. Meiss, J.; Allinger, N.; Riede, M. K.; Leo, K. *Appl. Phys. Lett.* **2008**, *93*, 103311.
56. Meiss, J.; Furno, M.; Pfuetzner, S.; Leo, K.; Riede, M. *J. Appl. Phys.* **2010**, *107*, 053117.
57. Koeppe, R.; Hoeglinger, D.; Troshin, P. A.; Lyubovskaya, R. N.; Razumov, V. F.; Sariciftci, N. S. *Chemsuschem* **2009**, *2*, 309.
58. Andersson, B. V.; Huang, D. M.; Moule, A. J.; Inganäs, O. *Appl. Phys. Lett.* **2009**, *94*, 043302.
59. Ajuria, J.; Etxebarria, I.; Cambarau, W.; Munecas, U.; Tena-Zaera, R.; Carlos Jimeno, J.; Pacios, R. *Energy Environ. Sci.* **2011**, *4*, 453.
60. Meiss, J.; Riede, M. K.; Leo, K. *J. Appl. Phys.* **2009**, *105*, 063108.
61. Oyamada, T.; Sugawara, Y.; Terao, Y.; Sasabe, H.; Adachi, C. *Jpn. J. Appl. Phys. Part 1* **2007**, *46*, 1734.
62. Bernede, J. C.; Berredjem, Y.; Cattin, L.; Morsli, M. *Appl. Phys. Lett.* **2008**, *92*, 083304.
63. Angmo, D.; Hösel, M.; Krebs, F. C. *Sol. Energy Mater. Sol. Cells* **2012**, *107*, 329.
64. Lee, J.; Connor, S. T.; Cui, Y.; Peumans, P. *Nano Lett.* **2008**, *8*, 689.
65. De, S.; Coleman, J. N. *ACS Nano* **2010**, *4*, 2713.
66. Yang, L.; Zhang, T.; Zhou, H.; Price, S. C.; Wiley, B. J.; You, W. *ACS Appl. Mater. Interfaces* **2011**, *3*, 4075.
67. Gaynor, W.; Burkhard, G. F.; McGehee, M. D.; Peumans, P. *Adv. Mater.* **2011**, *23*, 2905.
68. Leem, D.; Edwards, A.; Faist, M.; Nelson, J.; Bradley, D. D. C.; de Mello, J. C. *Adv. Mater.* **2011**, *23*, 4371.
69. Ajuria, J.; Ugarte, I.; Cambarau, W.; Etxebarria, I.; Tena-Zaera, R.; Pacios, R. *Sol. Energy Mater. Sol. Cells* **2012**, *102*, 148.
70. Morgenstern, F. S. F.; Kabra, D.; Massip, S.; Brenner, T. J. K.; Lyons, P. E.; Coleman, J. N.; Friend, R. H. *Appl. Phys. Lett.* **2011**, 99, 183307.
71. De, S.; Higgins, T. M.; Lyons, P. E.; Doherty, E. M.; Nirmalraj, P. N.; Blau, W. J.; Boland, J. J.; Coleman, J. N. *ACS Nano* **2009**, *3*, 1767.
72. Tokuno, T.; Nogi, M.; Karakawa, M.; Jiu, J.; Thi Thi Nge; Aso, Y.; Suganuma, K. *Nano Res.* **2011**, *4*, 1215.
73. Wu, J.; Hsu, S. L.; Tsai, M.; Liu, Y.; Hwang, W. *J. Mater. Chem.* **2012**, *22*, 15599.
74. Spechler, J. A.; Arnold, C. B. *Appl. Phys. A* **2012**, *108*, 25.
75. Hecht, D. S.; Hu, L.; Irvin, G. *Adv. Mater.* **2011**, *23*, 1482.
76. Shim, B. S.; Tang, Z.; Morabito, M. P.; Agarwal, A.; Hong, H.; Kotov, N. A. *Chem. Mater.* **2007**, *19*, 5467.
77. Zhou, Y. X.; Hu, L. B.; Gruner, G. *Appl. Phys. Lett.* **2006**, *88*, 123109.
78. Hatton, R. A.; Miller, A. J.; Silva, S. R. P. *J. Mater. Chem.* **2008**, *18*, 1183.
79. Dillon, A. C. *Chem. Rev.* **2010**, *110*, 6856.
80. Gruner, G. *J. Mater. Chem.* **2006**, *16*, 3533.
81. Lee, K.; Wu, Z.; Chen, Z.; Ren, F.; Pearton, S. J.; Rinzler, A. G. *Nano Lett.* **2004**, *4*, 911.
82. Wu, Z. C.; Chen, Z. H.; Du, X.; Logan, J. M.; Sippel, J.; Nikolou, M.; Kamaras, K.; Reynolds, J. R.; Tanner, D. B.; Hebard, A. F.; Rinzler, A. G. *Science* **2004**, *305*, 1273.
83. Pasquier, A. D.; Unalan, H. E.; Kanwal, A.; Miller, S.; Chhowalla, M. *Appl. Phys. Lett.* **2005**, *87*, 1.
84. Rowell, M. W.; Topinka, M. A.; McGehee, M. D.; Prall, H.; Dennler, G.; Sariciftci, N. S.; Hu, L.; Gruner, G. *Appl. Phys. Lett.* **2006**, *88*, 233506.

85. van de Lagemaat, J.; Barnes, T. M.; Rumbles, G.; Shaheen, S. E.; Coutts, T. J.; Weeks, C.; Levitsky, I.; Peltola, J.; Glatkowski, P. *Appl. Phys. Lett.* **2006**, *88*, 233503.

86. Ulbricht, R.; Lee, S. B.; Jiang, X.; Inoue, K.; Zhang, M.; Fang, S.; Baughman, R. H.; Zakhidov, A. A. *Sol. Energy Mater. Sol. Cells* **2007**, *91*, 416.

87. Tenent, R. C.; Barnes, T. M.; Bergeson, J. D.; Ferguson, A. J.; To, B.; Gedvilas, L. M.; Heben, M. J.; Blackburn, J. L. *Adv. Mater.* **2009**, *21*, 3210.

88. Barnes, T. M.; Bergeson, J. D.; Tenent, R. C.; Larsen, B. A.; Teeter, G.; Jones, K. M.; Blackburn, J. L.; van de Lagemaat, J. *Appl. Phys. Lett.* **2010**, *96*, 243309.

89. Kim, S.; Wang, X.; Yim, J. H.; Tsoi, W. C.; Kim, J.; Lee, S.; deMello, J. C. *J. Photonics Energy* **2012**, *2*, 021010.

90. Nirmalraj, P. N.; Lyons, P. E.; De, S.; Coleman, J. N.; Boland, J. J. *Nano Lett.* **2009**, *9*, 3890.

91. Ulbricht, R.; Jiang, X.; Lee, S.; Inoue, K.; Zhang, M.; Fang, S.; Baughman, R.; Zakhidov, A. *Phys. Status Solidi B* **2006**, *243*, 3528.

92. Zhang, M.; Fang, S. L.; Zakhidov, A. A.; Lee, S. B.; Aliev, A. E.; Williams, C. D.; Atkinson, K. R.; Baughman, R. H. *Science* **2005**, *309*, 1215.

93. Li, Z.; Kandel, H. R.; Dervishi, E.; Saini, V.; Xu, Y.; Biris, A. R.; Lupu, D.; Salamo, G. J.; Biris, A. S. *Langmuir* **2008**, *24*, 2655.

94. Kim, S.; Yim, J.; Wang, X.; Bradley, D. D. C.; Lee, S.; deMello, J. C. *Adv. Funct. Mater.* **2010**, *20*, 2310.

95. Geim, A. K.; Novoselov, K. S. *Nat. Mater.* **2007**, *6*, 183.

96. Bonaccorso, F.; Sun, Z.; Hasan, T.; Ferrari, A. C. *Nat. Photonics* **2010**, *4*, 611.

97. Pang, S.; Hernandez, Y.; Feng, X.; Muellen, K. *Adv. Mater.* **2011**, *23*, 2779.

98. Bae, S.; Kim, H.; Lee, Y.; Xu, X.; Park, J.; Zheng, Y.; Balakrishnan, J.; Lei, T.; Kim, H. R.; Song, Y. I.; Kim, Y.; Kim, K. S.; Özyilmaz, B.; Ahn, J.; Hong, B. H.; Iijima, S. *Nat. Nanotechnol.* **2010**, *5*, 574.

99. Kang, J.; Hwang, S.; Kim, J. H.; Kim, M. H.; Ryu, J.; Seo, S. J.; Hong, B. H.; Kim, M. K.; Choi, J. *ACS Nano* **2012**, *6*, 5360.

100. Park, H.; Brown, P. R.; Buloyic, V.; Kong, J. *Nano Lett.* **2012**, *12*, 133.

101. Wu, J.; Becerril, H. A.; Bao, Z.; Liu, Z.; Chen, Y.; Peumans, P. *Appl. Phys. Lett.* **2008**, *92*, 263302.

102. Kim, K. S.; Zhao, Y.; Jang, H.; Lee, S. Y.; Kim, J. M.; Kim, K. S.; Ahn, J.; Kim, P.; Choi, J.; Hong, B. H. *Nature* **2009**, *457*, 706.

103. Huang, X.; Yin, Z.; Wu, S.; Qi, X.; He, Q.; Zhang, Q.; Yan, Q.; Boey, F.; Zhang, H. *Small* **2011**, *7*, 1876.

104. Jo, G.; Choe, M.; Lee, S.; Park, W.; Kahng, Y. H.; Lee, T. *Nanotechnology* **2012**, *23*, 112001.

105. Wang, X.; Zhi, L.; Muellen, K. *Nano Lett.* **2008**, *8*, 323.

106. De Arco, L. G.; Zhang, Y.; Schlenker, C. W.; Ryu, K.; Thompson, M. E.; Zhou, C. *ACS Nano* **2010**, *4*, 2865.

107. Wang, Y.; Chen, X.; Zhong, Y.; Zhu, F.; Loh, K. P. *Appl. Phys. Lett.* **2009**, *95*, 063302.

108. Wang, Y.; Tong, S. W.; Xu, X. F.; Özyilmaz, B.; Loh, K. P. *Adv. Mater.* **2011**, *23*, 1514.

109. Kim, K. K.; Reina, A.; Shi, Y.; Park, H.; Li, L.; Lee, Y. H.; Kong, J. *Nanotechnology* **2010**, *21*, 285205.

110. Park, H.; Rowehl, J. A.; Kim, K. K.; Bulovic, V.; Kong, J. *Nanotechnology* **2010**,21.

111. Choe, M.; Lee, B. H.; Jo, G.; Park, J.; Park, W.; Lee, S.; Hong, W.; Seong, M.; Kahng, Y. H.; Lee, K.; Lee, T. *Org. Electron.* **2010**, *11*, 1864.

112. Larsen-Olsen, T. T.; Søndergaard, R. R.; Norrman, K.; Jørgensen, M.; Krebs, F. C. *Energy Environ. Sci.* **2012**, *5*, 9467.

113. Krebs, F. C.; Gevorgyan, S. A.; Alstrup, J. *J. Mater. Chem.* **2009**, *19*, 5442.

114. Krebs, F. C.; Nielsen, T. D.; Fyenbo, J.; Wadstrøm, M.; Pedersen, M. S. *Energy Environ. Sci.* **2010**, *3*, 512.

115. Krebs, F. C.; Fyenbo, J.; Jørgensen, M. *J. Mater. Chem.* **2010**, *20*, 8994.

116. Krebs, F. C.; Fyenbo, J.; Tanenbaum, D. M.; Gevorgyan, S. A.; Andriessen, R.; van Remoortere, B.; Galagan, Y.; Jørgensen, M. *Energy Environ. Sci.* **2011**, *4*, 4116.

117. Angmo, D.; Larsen-Olsen, T. T.; Jørgensen, M.; Søndergaard, R. R.; Krebs, F. C. *Adv. Energy Mater.* to apprear.